Applied Catalysis A: General 393 (2011) 153–160

Contents lists available at ScienceDirect

Applied Catalysis A: General

journal homepage: www.elsevier.com/locate/apcata

New mesoporous perovskite $ZnTiO_3$ and its excellent catalytic activity in liquid phase organic transformations

Nabanita Pal, Manidipa Paul, Asim Bhaumik*

Department of Materials Science, Indian Association for the Cultivation of Science, 2A & B Raja S. C. Mullick Road, Jadavpur, Kolkata 700 032, India

ARTICLE INFO

Article history:
Received 8 September 2010
Received in revised form
19 November 2010
Accepted 22 November 2010
Available online 27 November 2010

Keywords:
Liquid phase catalysis
Mesoporous materials
Perovskite
$ZnTiO_3$

ABSTRACT

A new mesoporous perovskite $ZnTiO_3$ material has been synthesized by the evaporation-induced self-assembly (EISA) method using non-ionic surfactant Pluronic P123 as template. After calcination of the dried gel of equimolar concentrations of Zn(II) and Ti(IV) at 673 K, a new perovskite mesophase of $ZnTiO_3$ (MZT-11) formed, having highly crystalline cubic $ZnTiO_3$ pore wall. Interestingly, in the absence of P123 but otherwise identical synthesis conditions showed no cubic structure and a mixed phase consisting of ZnO and TiO_2 phases (ZT-11). The BET surface area of the mesoporous perovskite materials (MZT-11) was 136 $m^2 g^{-1}$ and the average dimension of the pores was *ca.* 5.1 nm. The material was thoroughly characterized by different analytical methods including small and wide angle powder XRD, FE SEM, TEM, FT IR, UV–visible, photoluminescence (PL) and X-ray fluorescence (XRF) analysis. This new mesoporous perovskite material showed excellent catalytic activity in the Friedel-Crafts (FC) benzylation of aromatics and in the Fischer esterification of different long chain carboxylic acids in the presence of methanol under solvent-free conditions.

1. Introduction

Crystalline ceramics mainly perovskite-type mixed metal oxides of chemical formula ABO_3 have attracted keen interest over the years owing to their unique physical and chemical properties [1]. Their physical properties (dielectric, ferroelectric etc.) are exploited in electrical and optical applications along with their chemical properties, including their potential in the generation of thermoelectric power [2]. ABO_3-type perovskites are mixed oxides having BO_6 octahedra with A^{2+} cations inserted in the framework. Titanium-based perovskite oxides of $A^{II}Ti^{IV}O_3$ type, where A is Pb, Sr, Ba, Zn or Fe, have attracted wide-spread attention in different frontier areas of research due to their outstanding potential in electronics [3], semiconductor [4], solid oxide fuel cell (SOFC) [5], gas sensors [6], memory devices [7], magnetic materials [8], photocatalysis [9] and heterogeneous catalysis [10]. However, there are only very few reports on the liquid phase heterogeneous acid catalyzed reactions over these perovskite oxides.

In addition, when a perovskite type multimetal oxide attains mesoporosity with appreciably good surface area, it can play a key role in gas storage [11], ion-exchange [12], adsorption [13], ion-conduction [14] or catalysis [15] based on the nature of the hetero atoms. Since the discovery of MCM-41/48 by Mobil researchers [16], a large variety of mesoporous materials, including silica based organic–inorganic hybrid materials [17–22], non-siliceous mesoporous metal oxides [23], phosphates [24] and organic polymers [25] have been studied intensively due to their versatile applications. However, in this context very little attention has been paid to the synthesis of mesoporous mixed metal oxides and their application potentials [26–28]. This may be due to the lack of phase purity [29] and the low thermal stability during synthesis of those materials. The removal of template from the as-synthesized mesoporous mixed metal oxide composites through solvent extraction in many instances causes collapse of the mesophases. From these circumstances a pure phase can only be generated at very high temperature calcination. But this may result in reduction of the surface area and often in loss of mesoporosity. Thus the synthesis of pure mesoporous perovskite type mixed oxide is a great challenge. Titanium containing mixed perovskite oxide is generally synthesized via sol–gel method [30] or solid state reactions [31]. But the evaporation-induced self-assembly (EISA) method [32] has been rarely employed in the synthesis of mixed oxides as there is a possibility of heterogeneity in the reaction medium due to the rapid hydrolysis and coagulation at the time of solvent evaporation.

Nonporous perovskite $ZnTiO_3$ has been employed as catalyst in various organic reactions like dehydrogenation reactions [33] as well as in the detoxification of chemicals [34,35]. Although mesoporous zinc oxide-layered titanate nanocomposites, a closely related material, have been synthesized by an exfoliation-restacking route [36] and possess good surface areas, but to the best of our knowledge the pure mesoporous perovskite $ZnTiO_3$ has not been reported so far. Further, nonporous $ZnTiO_3$ perovskite oxide

* Corresponding author. Tel.: +91 33 2473 4971.
E-mail address: msab@iacs.res.in (A. Bhaumik).

0926-860X/$ – see front matter © 2010 Elsevier B.V. All rights reserved.
doi:10.1016/j.apcata.2010.11.037

is usually synthesized through a high temperature mixed-oxide method. Herein, we wanted to explore the possibility of the synthesis of mesoporous $ZnTiO_3$ through solution phase low temperature evaporation-induced self-assembly (EISA) method via a surfactant templating pathway. Our synthesis strategy for the preparation of this material is energy saving and this method introduces mesoporosity, which can enhance the surface properties of the material. Herein, we first synthesized mesoporous $ZnTiO_3$ material having cubic perovskite structure through EISA method. Moreover, the material exhibits good efficiency as heterogeneous catalyst in liquid phase acid catalyzed Friedel-Crafts benzylation and Fischer esterification reactions. Both these reactions are commercially practiced organic reactions [37,38]. Alkylation of benzene and substituted benzenes by benzyl chloride produces a variety of important fine chemicals, which have many useful applications in designing drug molecules. On the other hand, carboxylic acid esters are widely used in numerous cases like biodiesel fuel, detergents, and emulsification. FC benzylation or esterification reactions in the presence of homogeneous catalysts like $AlCl_3$ or H_2SO_4 although giving better yields in industrial scale [39]; these catalysts, however, have severe drawbacks such as difficulty of separation and handling, corrosiveness, toxicity, etc. Thus, we need a non-corrosive, non-toxic, reusable heterogeneous solid catalyst, which can be synthesized in a convenient, cost-effective and environment friendly route [40]. In this context, successful synthesis and utilization of mesoporous perovskite $ZnTiO_3$ material is very much important.

2. Experimental

2.1. Materials

Poly(ethylene glycol)-*block*-poly(propylene glycol)-*block*-poly (ethylene glycol), Pluronic P123 (M_{av} = 5800, $EO_{20}PO_{70}EO_{20}$, template) and titanium(IV) isopropoxide (Ti-precursor) were purchased from Sigma–Aldrich. $Zn(NO_3)_2{\cdot}6H_2O$, concentrated HCl (35%), benzene, toluene, *p*-xylene, benzyl chloride, methanol, and oleic acid were purchased from Merck, India. Palmitic and lauric acid were purchased from Loba Chemie, India. Ethyl alcohol (absolute ethanol) AR.99.9% was received from Changshu Yangyuan Chemical, China. Water used was distilled water manufacturer company Broadway chemicals (India). PE film was purchased from Parafilm "M" of American National Can. All the chemicals were used as received.

2.2. Synthetic procedure

In a typical synthesis (for MZT-11), 1.0 g of Pluronic P123 was dissolved in a mixture of 20 ml of ethanol and 1.2 g of concentrated HCl at room temperature with 1 h continuous stirring. Then 3.0 g of zinc nitrate was added to this solution. After half an hour stirring, 2.85 g of titanium isopropoxide was mixed with the clear sol solution. The mixture was kept under stirring at RT for another 5–6 h covering with small pieces (70 mm × 80 mm) of PE (polyethylene) film. Gradually a white gel was formed, which was aged at RT for 3 days in a slow evaporation process followed by slow heating at 333 K for 4 days. The white solid formed was calcined at 673 K for 4 h in air to remove the Pluronic P123 template. Similarly, a reference non porous Zn–Ti mixed oxide sample was synthesized under identical conditions in the absence of Pluronic P123 template. The white solid obtained has been designated ZT-11.

2.3. Characterization methods

Powder X-ray diffraction (XRD) patterns of the materials were recorded on a Bruker AXS D-8 Advance diffractometer operated at 40 kV voltage and 40 mA current and calibrated with a standard silicon sample, using Ni-filtered Cu K_α (λ = 0.15406 nm) radiation. Nitrogen adsorption/desorption isotherms were obtained using a Beckmann Coulter SA 3100 surface area analyzer at 77 K. Prior to the measurement, all the samples were degassed at 453 K for 3 h. TEM images were recorded by a JEOL JEM 2010 transmission electron microscope. A JEOL JEM 6700F field emission scanning electron microscope with an energy dispersive X-ray spectroscopic (EDS) attachment was used to record SEM images of the sample and its surface chemical composition. Fourier transform infrared (FT IR) spectra of these samples on KBr pellets were recorded by using a Shimadzu FT IR 8300 spectrophotometer. Thermogravimetry (TG) study and differential thermal analysis (DTA) were carried out on a TA instrument Q600 DSC/TGA thermal analyzer. For optical measurement, each powder sample was pressed into the sample holder carefully. UV–visible diffuse reflectance spectra were obtained by using a Shimadzu UV 2401PC spectrophotometer with an integrating sphere attachment; a $BaSO_4$ pellet was used as background standard. A high-resolution Perkin Elmer LS 55 luminescence spectrometer was used to detect the photoluminescence (PL) from the sample. Energy dispersive X-ray fluorescence spectroscopic (EDXRF) analysis was done using an in-house developed set-up consisting of a 109Cd source (AEA technologies, 4 mm dia and 115 MBq effective activity) and a Si(Li) detector (Canberra, 8 μm Be window, 30 mm^2 active area, 5 mm effective thickness, and 145 eV resolution or FWHM at 5.9 keV). The detection medium was air with an X-ray detection range of 3–20 keV. The spectrum analysis and quantification was done using the AXIL-QXAS code (IAEA).

2.4. Catalytic methods

Liquid phase Friedel-Crafts (FC) benzylation reactions were carried out with benzene or substituted aromatics as substrates in a two-necked round bottom flask fitted with a water condenser and placed in an oil bath at 343–348 K temperature under stirring. We have preheated the as-prepared powder samples at 423 K for 2 h before conducting the liquid phase catalytic reactions. Benzylating agent benzyl chloride had been added at the start of the reaction, keeping the ratio of substrate:reagent = 10:1. This is followed by the addition of our solid mesoporous catalyst in required amount. At different time intervals the products were collected from the reaction mixture and analyzed by capillary gas chromatography (Agilent 7890D, FID). The products were identified by using known standards.

The Fischer esterification reactions of different carboxylic acids (CA) were carried out in the same equipment at 333 K taking dry methanol in CA:methanol = 1:120 molar ratio. The required amount of each catalyst was added to it under continuous stirring in the presence of 0.3 g of molecular sieves. After the reaction was completed, solid catalyst was filtered and the methanol was removed through a rotary evaporator. The products were identified by FT NMR and the percentage of conversion was measured by acid–base titration method using 0.001 N NaOH solution. ^1H and ^{13}C NMR experiments were carried out on a Bruker DPX-300 NMR spectrometer.

3. Results and discussions

3.1. Chemical composition

The surface composition of the as-synthesized and calcined MZT-11 is estimated by XRF analysis (Table 1). It reveals that the ratio of Zn:Ti is 1:1.02 in MZT-11, which is almost the same as the composition of the reaction mixture gel. Thus the stoichiometry of this novel mesoporous material resembles well a unimolar ratio of Zn and Ti in $ZnTiO_3$.

Table 1
Chemical composition of mesoporous perovskite $ZnTiO_3$.

Sample name	Element	Atomic % (from EDS data)	Ratio of Zn:Ti	wt% (from XRF data)	Ratio of Zn:Ti
MZT-11	Ti Zn	18.31 17.99	1:1.02	34.4 ± 0.1 32.0 ± 0.3	1:1.075

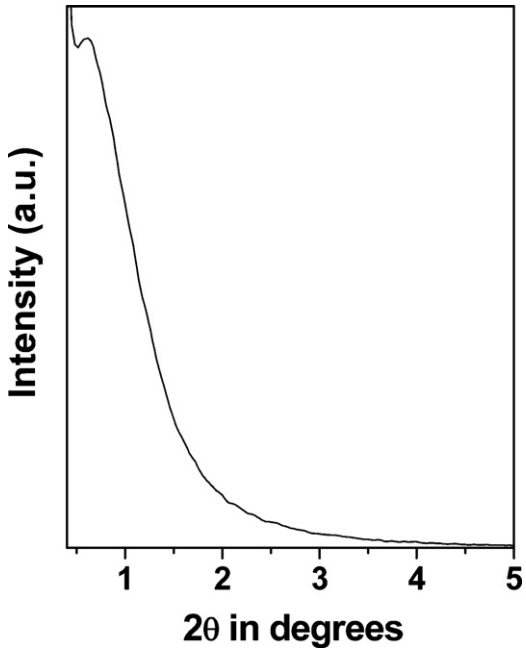

Fig. 1. Small angle powder XRD patterns of calcined MZT-11.

3.2. Nanostructure

The small angle powder XRD pattern of the calcined MZT-11 is shown in Fig. 1. The material exhibit a broad peak near $2\theta = 0.61^\circ$. The 2θ values correspond to the inter-pore separation of 14.5 nm. This result suggested that our mesoporous perovskite $ZnTiO_3$ material has nanostructure consisting of disordered mesophases with no short or long range ordering. In Fig. 2A the wide angle XRD pattern

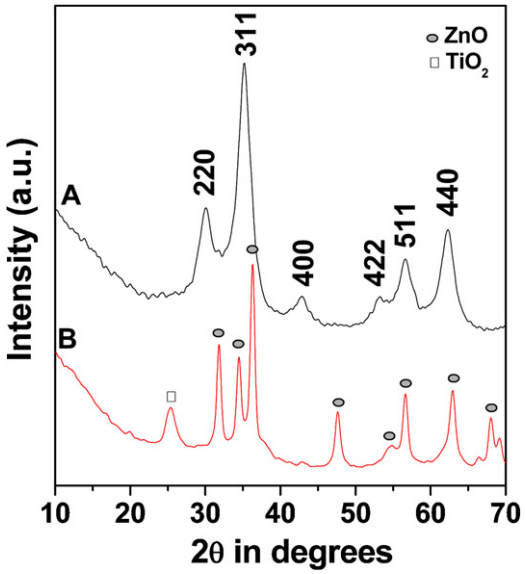

Fig. 2. Wide angle powder XRD of calcined MZT-11 (A) and ZT-11 (B) samples.

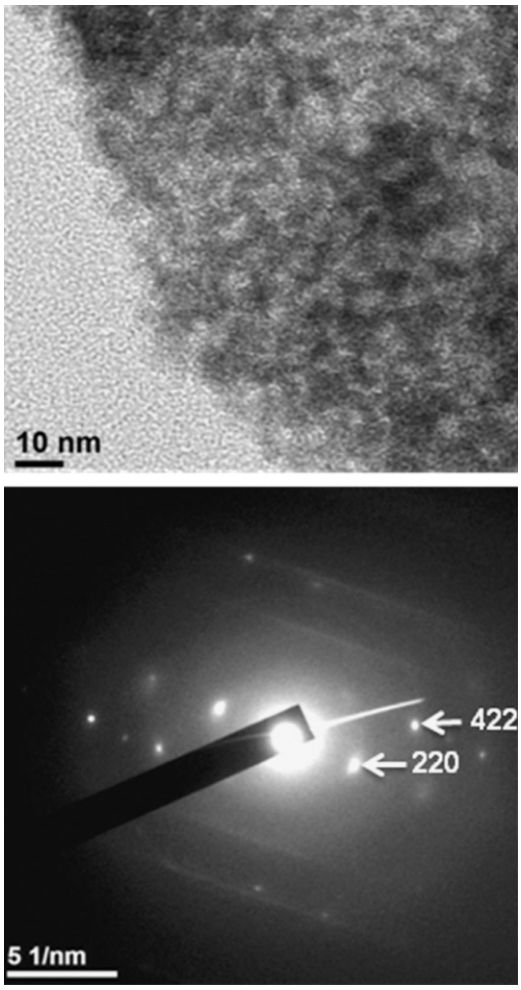

Fig. 3. HRTEM image of mesoporous MZT-11 (upper) and corresponding selected area electron diffraction (SAED) pattern (lower).

of MZT-11 is shown. The material showed good crystallinity having a good correspondence with the XRD pattern of cubic perovskite $ZnTiO_3$ structure (JCPDS file no. 39-0190) [41]. Major diffraction peaks agree very well with the (2 2 0), (3 1 1), (4 0 0), (4 2 2), (5 1 1) and (4 4 0) planes and can be indexed to a cubic phase of $ZnTiO_3$. The lattice parameter of the cubic unit cell is $a = b = c = 0.841$ nm (as per the JCPDS data) [41]. The mean size of the crystalline domain (calculated using the Scherrer equation) from the high angle XRD pattern suggests *ca.* 5.05 nm grain size. Very broad and moderate intensity peaks with preferential growth of (3 1 1) cubic phase of perovskite $ZnTiO_3$ has been clearly observed here [41]. No peak corresponding to the ZnO, TiO_2 or zinc titanates of other stoichiometries (α-Zn_2TiO_4 or $Zn_2Ti_3O_8$) [42] is observed. Further, there is hardly any resemblance of this wide angle powder XRD pattern to that of hexagonal form of ilmenite $ZnTiO_3$ [43]. Thus it is clear that a 1:1 molar ratio in the synthetic gel is properly maintained in the stoichiometric ratio of MZT-11 and that the pore walls of this novel mesoporous material consist of crystalline $ZnTiO_3$ domains. Fig. 2B exhibits the XRD pattern of nonporous mixed oxide sample ZT-11, which is a mixed phase of individual ZnO and TiO_2 synthesized in the absence of Pluronic P123. Crystalline domain size calculated is 13.3 nm, i.e. the grain size is much larger than that of MZT-11. Thus it is evident from high angle powder XRD that cubic perovskite $ZnTiO_3$ phase does not form in the absence of a Pluronic template and such low calcination temperature. In Fig. 3 HR TEM images of our mesoporous perovskite $ZnTiO_3$ material are shown. As seen from these images, these mesopores are disordered wormhole-

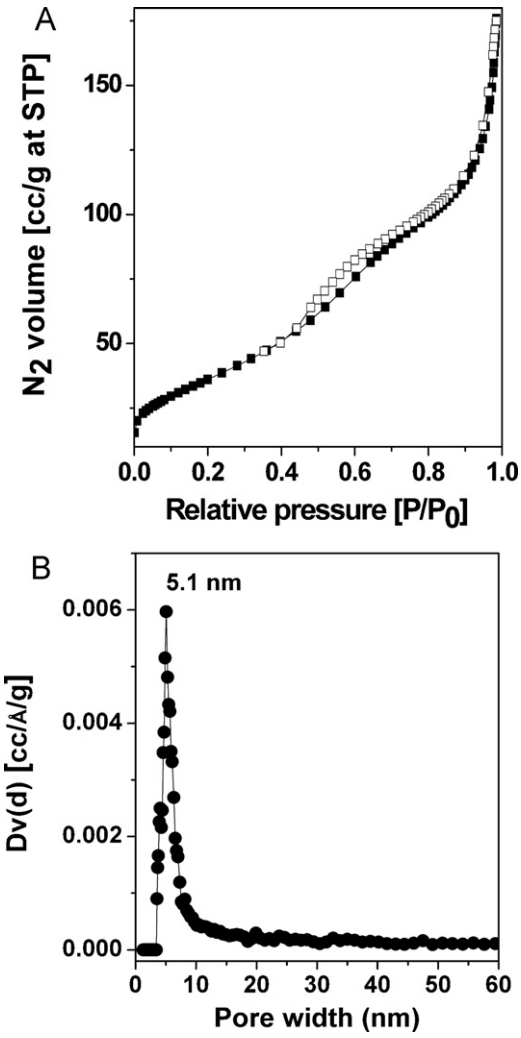

Fig. 4. (A) N_2 adsorption (■)–desorption (□) isotherms of MZT-11 measured at 77 K. (B) Corresponding pore size distribution using NLDFT method.

like in nature [44,45]. The dimension of the pores varies around 5.0–5.5 nm. Hence the porosity is generated due to interparticle spacing of $ZnTiO_3$ nanoparticles. A close look to the image exhibits uniform distribution of particles with *ca.* 5.0 nm size. The SAED pattern shown in the inset of this figure also resembles closely the cubic perovskite $ZnTiO_3$ structure.

3.3. Mesoporosity

In Fig. 4 we have plotted the N_2 adsorption–desorption isotherms of the calcined MZT-11 material at liquid nitrogen temperature (77 K). Typical type IV isotherms with H1 type hysteresis loops at high P/P_0 value are observed, characteristic of large mesopores [45]. More specifically the mesoporosity coming up due to the interparticle voids of large numbers of very small particles distributed throughout the specimen is responsible for the vertical slope at high P/P_0 region. The BET surface area of MZT-11 was 136 $m^2\,g^{-1}$ together with a pore volume of 0.23 $cm^3\,g^{-1}$; whereas the surface area of ZT-11 was only 56 $m^2\,g^{-1}$ (isotherm not shown). From the isotherms in Fig. 4B we have plotted the pore size distribution employing NLDFT (Non-Local Density Functional Theory) method [46]. The material MZT-11 showed a very narrow pore size distribution with peak maxima centered at *ca.* 5.1 nm.

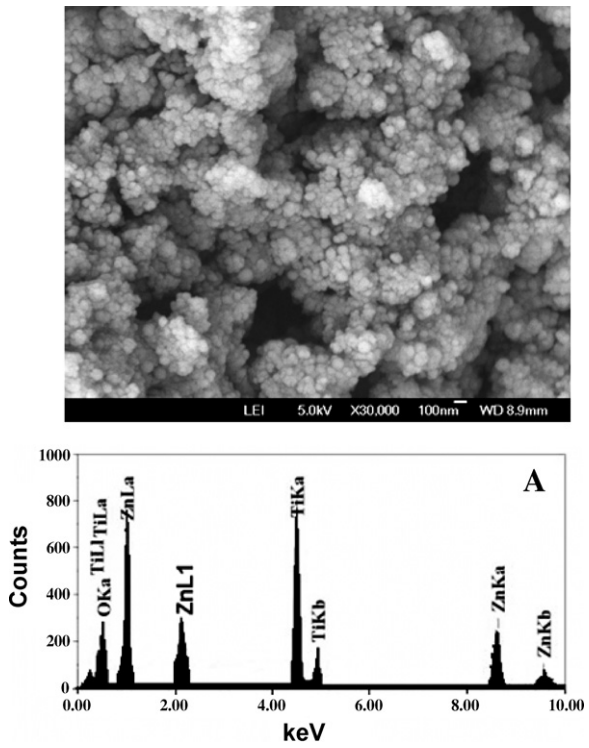

Fig. 5. FE SEM image of calcined MZT-11 material. (A) EDS pattern of mesoporous MZT-11.

3.4. Morphology

The FE SEM image (Fig. 5) of our mesoporous perovskite $ZnTiO_3$ material shows a uniform distribution of tiny spherical particles. In some parts of the specimen these nanoparticles are self-assembled to form large aggregates. The EDS chemical analysis plot of mesoporous perovskite $ZnTiO_3$ is shown in Fig. 5A. Chemical composition obtained from EDS agrees very well with the XRF result (Table 1).

3.5. Framework and bonding

Infrared spectra of the as-synthesized and calcined MZT-11 samples are shown in Fig. 6. The absence of any peak for a C–H bond near 3000 cm^{-1} in the calcined mesoporous perovskite $ZnTiO_3$ material suggests complete removal of organic Pluronic template after calcination. A broad band observed near 3425 cm^{-1} and 1618 cm^{-1} could be attributed to O–H stretching and H–O–H bending vibrations of the adsorbed water molecules. The absorption peak of –O–R bond around 1090 cm^{-1} in the as-synthesized sample disappears in the calcined one, which signifies the complete hydrolysis of titanium precursor during the EISA method. Peaks at 598 cm^{-1} and 438 cm^{-1} could be attributed to the stretching vibrations for the Ti–O and Zn–O bonds [47]. Thus the FT IR spectroscopic results suggested the presence of different framework vibrations in the mesoporous $ZnTiO_3$ material.

3.6. Optical measurements

The UV–visible absorption spectrum of mesoporous perovskite $ZnTiO_3$ sample is shown in Fig. 7. The figure indicates that the material shows absorption maxima *ca.* 265 nm and a shoulder at *ca.* 363 nm. These absorption bands are considerably different from those of anatase TiO_2 [48] and wurzite ZnO [49] and agree well with the nonporous perovskite $ZnTiO_3$ [50]. On the other hand the

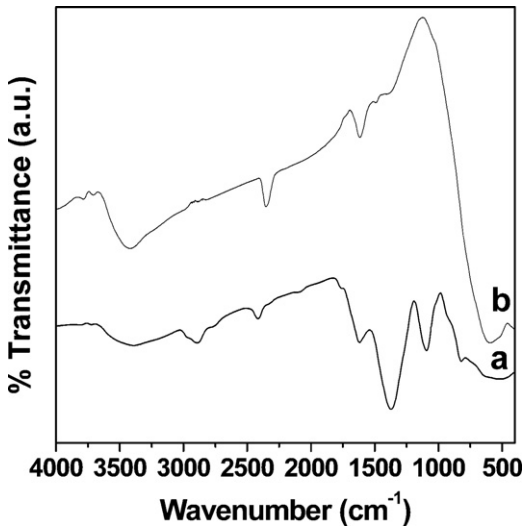

Fig. 6. FTIR spectrum of as-synthesized (a) and calcined (b) MZT-11.

absorption spectrum of ZT-11 showed a quite different pattern. The features of both oxides ZnO and TiO_2 in sample ZT-11 are reflected in high intensity peaks at *ca.* 365 nm and 315 nm, respectively. The direct optical band gaps estimated from the absorption spectra for the sample MZT-11 and ZT-11 are shown in Fig. 8A and B. An optical band gap is obtained by plotting $(\alpha h\nu)^2$ vs $h\nu$ where α is the absorption co-efficient and $h\nu$ is photon energy. Extrapolation of the linear portion at $(\alpha h\nu)^2 = 0$ gives the band gaps of 3.59 eV for our mesoporous perovskite $ZnTiO_3$ material and 3.07 eV for the ZnO–TiO_2 mixed oxide sample. The optical band gap of MZT-11 is smaller than those of the nonporous $ZnTiO_3$ (band gap 3.70 eV) thin films obtained by radio frequency cosputtering of ZnO and TiO_2 [51]. Thus, for our mesoporous $ZnTiO_3$ mixed oxide, the minimum energy required for the excitation of an electron from valence to conduction band is considerably higher than that required for the pure anatase TiO_2 and ZnO (*ca.* 3.2 eV). The room temperature photoluminescence (PL) spectrum of our mesoporous perovskite

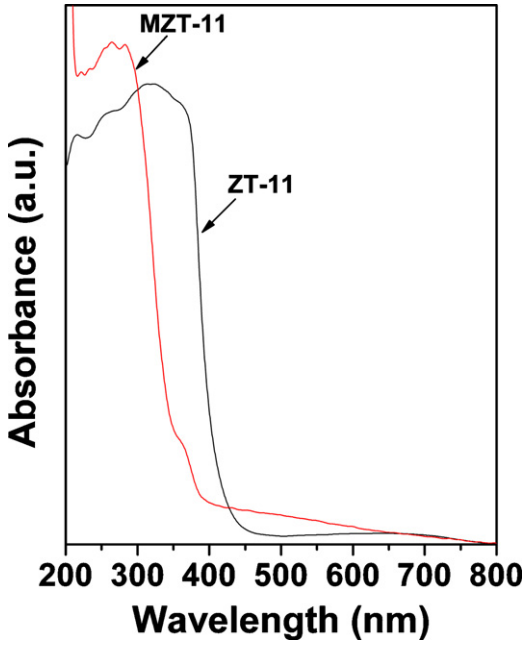

Fig. 7. UV–visible diffuse reflectance spectra of mesoporous perovskite MZT-11 and ZT-11.

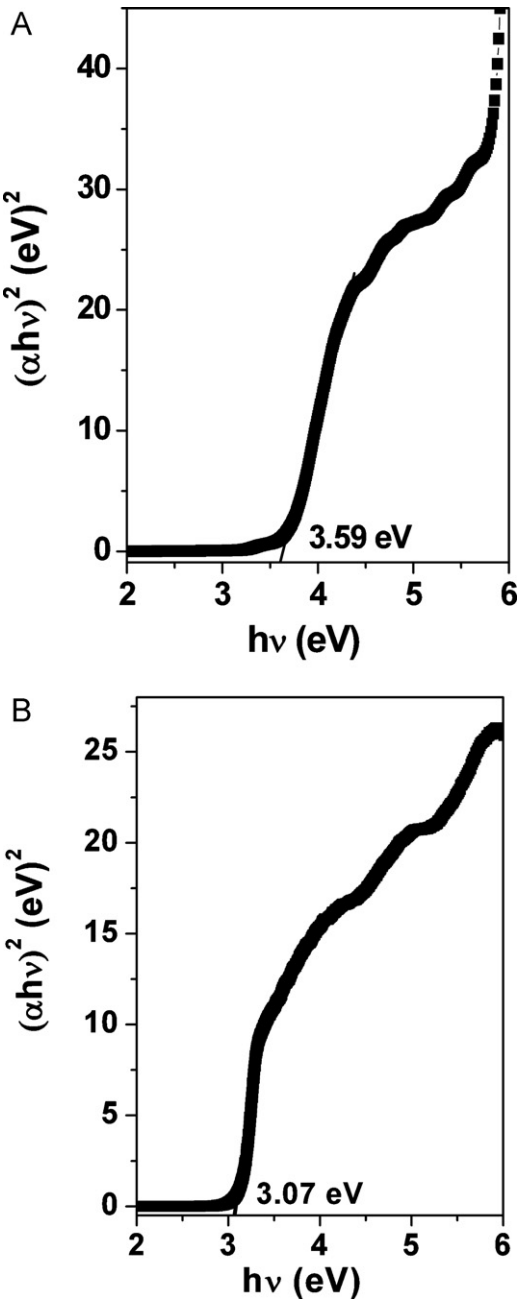

Fig. 8. Estimated band gap of MZT-11 (A) and ZT-11 (B) materials.

$ZnTiO_3$ sample is shown in Fig. 9. The material shows a very broad and strong photoluminescence band centered at 390 nm and one weak emission peak at 419 nm upon excitation at 270 nm. These emission bands are not band to band transitions because the peak positions (390 nm, 3.18 eV) and (419 nm, 2.96 eV) are much smaller than the optical band gap of the mesoporous $ZnTiO_3$ material (3.59 eV). The existence of intrinsic defect states in our mesoporous $ZnTiO_3$ material (synthesized in the presence of non-ionic template and calcined in air at 673 K) such as O^{2-} vacancy, Zn^{2+} interstitial and/or Zn^{2+} vacancy could be responsible for these UV and blue emissions [51].

3.7. Catalytic properties

The FC benzylation (Scheme 1) of different aromatic molecules over mesoporous perovskite $ZnTiO_3$ sample is shown in Table 2.

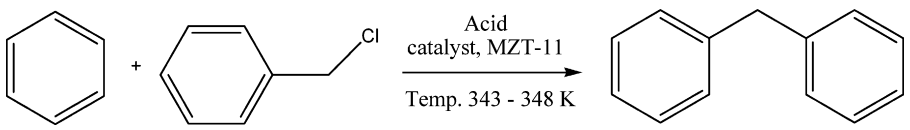

Scheme 1.

Table 2
Benzylation of different aromatics over MZT-11.[a]

Substrate	Product	Time (h)	Conversion (%)	Selectivity (%)
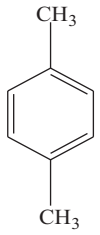	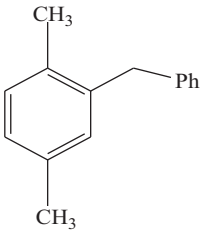	24	92.3	100
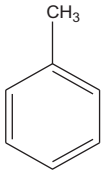	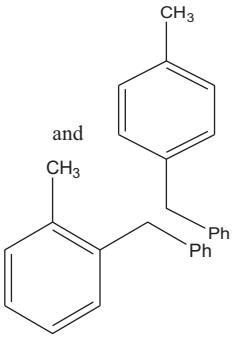	24	90.2	34.6 (*o*-product) 65.4 (*p*-product)
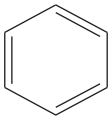	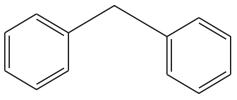	14	93.6	100

[a] Reaction conditions: temperature 348 K (for benzene 343 K), substrate:benzyl chloride = 10:1, catalyst 1 wt% of the total reactants.

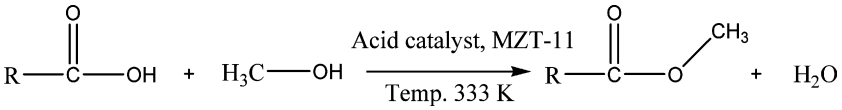

Scheme 2.

Table 3
Esterification of carboxylic acids (CAs) with methanol over MZT-11.[a]

Substrate (CA)	Product	Time (h)	Conversion (%)
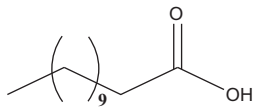	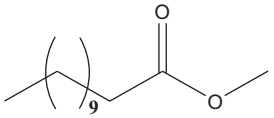	16	92.3
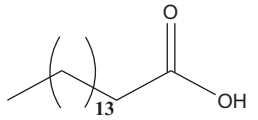	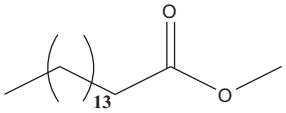	15	78.1
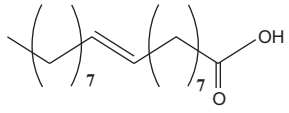	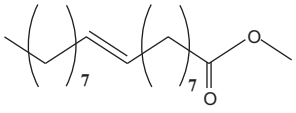	18	73.2

[a] Reaction conditions: CA:methanol = 1:120, temperature 333 K, catalyst 2 wt% with respect to the total reactants.

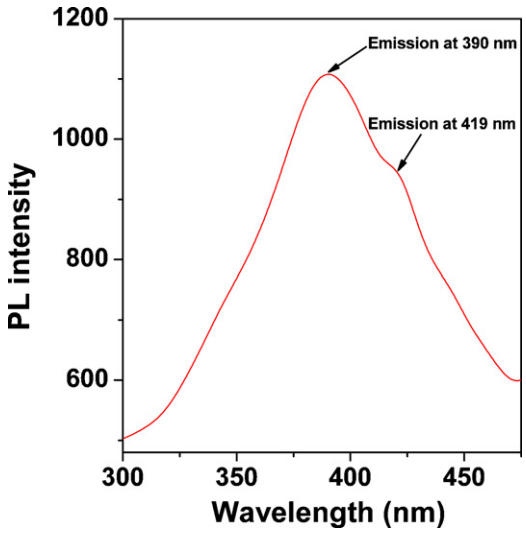

Fig. 9. Room temperature photoluminescence spectrum of mesoporous MZT-11 upon using 270 nm light excitation.

High conversion of benzene, toluene or *p*-xylene into their respective benzylated derivatives is observed together with high selectivity for monobenzylated product. For toluene the observed ratio of *p*-/*o*- benzylated isomers was *ca.* 2.0, suggesting considerable steric hindrance at the ortho position to the methyl group that could be attributed to low ortho-benzylation. The presence of strong Lewis acid sites at the surface could be responsible for this acid catalyzed reaction. On the other hand the esterification reaction (Scheme 2) is an important reaction for the production of biodiesels from the catalytic reaction of long chain fatty acids with aliphatic alcohols. In Table 3 we have summarized our results on the esterification of lauric, palmitic and oleic acids with methanol in the presence of mesoporous $ZnTiO_3$ material. Here we observed rather high yields of the corresponding methyl-esters (Table 3) [52]. As the aliphatic chain length of the monobasic acids increases from lauric < palmitic < oleic acid, the respective molecular mass increases and this is reflected in a consequent decrease in the esterification rate. In Scheme 3 we have shown a possible mechanism for the acid catalyzed esterification reaction. Initially, the carboxylic acid coordinates to the Lewis acidic site present at the catalyst surface (I). This is followed by an attack of an oxygen atom of the methanol molecule to the carbonyl carbon of (II). The active cationic species formed (III) immediately rearranges to eliminate the corresponding methyl-ester. The intermediate catalyst species (IV) regenerates the solid catalyst via elimination of one H_2O molecule. Molecular sieves added in the reaction medium removes these byproduct water molecules and accelerate the forward reaction. Thus it is clear that the presence of strong Lewis acid sites as well as a high surface area of the catalyst accelerates the reaction pathway. In the cases of higher molecular weight aliphatic compounds the –R group provide a steric hindrance to the incoming MeOH molecule, which could result in low conversion for the corresponding methyl-ester (Table 1).

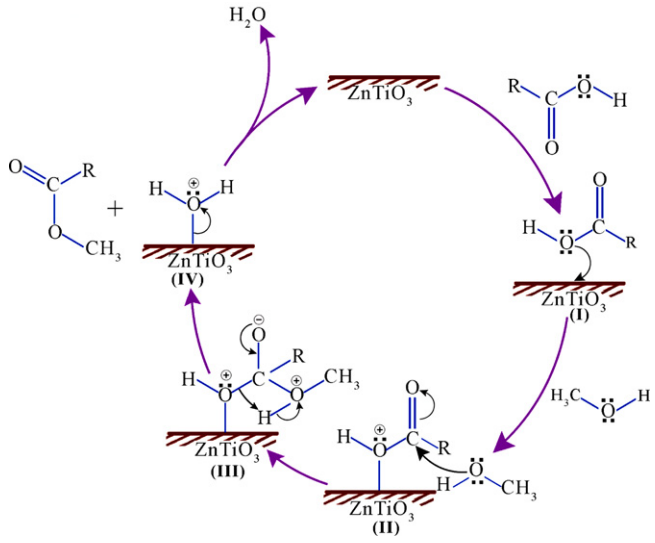

Scheme 3.

4. Conclusion

Mesoporous perovskite $ZnTiO_3$ having cubic pore wall structure has been synthesized using a non-ionic template Pluronic P123 through an evaporation-induced self-assembly method. The material exhibits high crystalline feature together with a moderately good surface area and narrow pore size distribution after the removal of the template molecules. With a similar synthetic strategy, applied without using Pluronic P123 as template, a mixed $ZnO–TiO_2$ phase material is formed having very poor surface area and no mesoporosity. This result suggested that Pluronic P123 plays a crucial role in the formation of cubic perovskite $ZnTiO_3$ structure with mesoporosity at a low calcinations temperature of 673 K. The novel mesoporous $ZnTiO_3$ material showed excellent catalytic efficiency in acid-catalyzed Friedel-Crafts benzylation and in Fischer esterification of many organic substrates under solvent-free condition. The high conversion rate observed in the esterification reactions can open up new potential applications of this mesoporous perovskite $ZnTiO_3$ material in the production of biodiesels with catalytic reactions of vegetable oils or animal fats having long chain aliphatic alcohols.

Acknowledgements

AB wishes to thank the Department of Science and Technology (DST), New Delhi for financial support. NP and MP are grateful to the Council of Scientific and Industrial Research (CSIR), New Delhi for their senior research fellowships. The authors also express their sincere thanks to Saha Institute of Nuclear Physics (SINP), Kolkata for providing the ED-XRF facility.

References

[1] C.D. Chandler, C. Roger, M.J. Hampden-Smith, Chem. Rev. 93 (1993) 1205–1241.
[2] I. Terasaki, M. Iwakawa, T. Nakano, A. Tsukuda, W. Kobayashi, Dalton Trans. 39 (2010) 1005–1011.
[3] S.-Y. Chung, I.-D. Kim, S.J.L. Kang, Nat. Mater. 3 (2004) 774–778.
[4] J.W. Fergus, Sens. Actuators B: Chem. 123 (2007) 1169–1179.
[5] J.C. Ruiz-Morales, J. Canales-Vazquez, C. Savaniu, D. Marrero-Lopez, P. Nunez, W.Z. Zhou, J.T.S. Irvine, Phys. Chem. Chem. Phys. 9 (2007) 1821–1830.
[6] I. Kosacki, H.U. Anderson, Sens. Actuators B: Chem. 48 (1998) 263–269.
[7] A. Sawa, Mater. Today 11 (2008) 28–36.
[8] Y.D. Yang, S. Priya, Y.U. Wang, J.F. Li, D. Viehland, J. Mater. Chem. 19 (2009) 4998–5002.
[9] X.K. Li, T. Kako, J.H. Ye, Appl. Catal. A: Gen. 326 (2007) 1–7.
[10] R. Horyn, R. Klimkiewicz, Appl. Catal. A: Gen. 370 (2009) 72–77.
[11] X. Hu, B.O. Skadtchenko, M. Trudeau, D.M. Antonelli, J. Am. Chem. Soc. 128 (2006) 11740–11741.
[12] M.J. Manos, K. Chrissafis, M.G. Kanatzidis, J. Am. Chem. Soc. 128 (2006) 8875–8883.
[13] J.M. Kisler, A. Dähler, A.W. Stevens, G.A.J. O'Connor, Microporous Mesoporous Mater. 44–45 (2001) 769–774.
[14] P. Knauth, Solid State Ionics 180 (2009) 14–16.
[15] R. Klimkiewicz, J. Trawczynski, Appl. Catal. A: Gen. 360 (2009) 199–204.
[16] C.T. Kresge, M.E. Leonowicz, W.J. Roth, J.C. Vartuli, J.S. Beck, Nature 359 (1992) 710–712.
[17] A. Corma, J.L. Jordá, M.T. Navarro, F. Rey, Chem. Commun. (1998) 1899–1900.
[18] A. Bhaumik, T. Tatsumi, J. Catal. 182 (2000) 31–39.

[19] D. Chandra, T. Yokoi, T. Tatsumi, A. Bhaumik, Chem. Mater. 19 (2007) 5347–5354.
[20] B. Camarota, B. Onida, Y. Goto, S. Inagaki, E. Garrone, Langmuir 23 (2007) 13164–13168.
[21] K. Sarkar, M. Nandi, M. Islam, T. Mubarak, A. Bhaumik, Appl. Catal. A: Gen. 352 (2009) 81–86.
[22] K.M. Parida, S. Singha, P.C. Sahoo, J. Mol. Catal. A: Chem. 325 (2010) 40–47.
[23] T. Brezesinski, M. Groenewolt, N. Pinna, H. Amenitsch, M. Antonietti, B.M. Smarsly, Adv. Mater. 18 (2006) 1827–1831.
[24] T. Kimura, Chem. Mater. 17 (2005) 337–344.
[25] D. Chandra, A. Bhaumik, J. Mater. Chem. 19 (2009) 1901–1907.
[26] D. Grosso, C. Boissiere, B.M. Smarsly, T. Brezesinski, N. Pinna, P.A. Albouy, H. Amenitsch, M. Antonietti, C. Sanchez, Nat. Mater. 3 (2004) 787–792.
[27] E.L. Crepaldi, G.J.D.A. Soler-Illia, A. Bouchara, D. Grosso, D. Durand, C. Sanchez, Angew. Chem. Int. Ed. 42 (2003) 347–351.
[28] R.Z. Hou, P. Ferreira, P.M. Vilarinho, Microporous Mesoporous Mater. 110 (2008) 392–396.
[29] Y. Narendar, G.L. Messing, Catal. Today 35 (1997) 247–268.
[30] O. Yamaguchi, M. Morimi, H. Kawabata, K. Shimizu, J. Am. Ceram. Soc. 70 (1987) C97–C98.
[31] J.M. Xue, D.M. Wan, S.E. Lee, J. Wang, J. Am. Ceram. Soc. 82 (1999) 1687–1692.
[32] C.J. Brinker, Y. Lu, A. Sellinger, H. Fan, Adv. Mater. 11 (1999) 579–585.
[33] Z.X. Chen, A. Derking, W. Koot, M.P. van Dijk, J. Catal. 161 (1996) 730–741.
[34] A. Chaouchi, S. d'Astorg, S. Marinel, M. Aliouat, Mater. Chem. Phys. 103 (2007) 106.
[35] G. Liu, G. Li, X. Qiu, L. Li, J. Alloys Compd. 481 (2009) 492.
[36] T.W. Kim, S.-J. Hwang, Y. Park, W. Choi, J.-H. Choy, J. Phys. Chem. C 111 (2007) 1658–1664.
[37] G.A. Olah, Friedel-Crafts Chemistry, Wiley, New York, 1973.
[38] S. Cotton, Educ. Chem. 34 (1997) 62.
[39] R. Commandeur, N. Berger, P. Jay, J. Kervenal, Eur. Pat., 0,422,986 (1991).
[40] N.R. Shiju, V.V. Guliants, Appl. Catal. A: Gen. 356 (2009) 1–17.
[41] A.R. Phani, M. Passacantando, S. Santucci, J. Phys. Chem. Solids 68 (2007) 317–323.
[42] M. Ocana, W.P. Hsu, E. Matijevic, Langmuir 7 (1991) 2911–2916.
[43] Y.L. Chai, Y.S. Chang, Y.J. Hsiao, Y.C. Lian, Mater. Res. Bull. 43 (2008) 257–263.
[44] D. Chandra, N. Mukherjee, A. Mondal, A. Bhaumik, J. Phys. Chem. C 112 (2008) 8668–8674.
[45] M. Paul, N. Pal, B.S. Rana, A.K. Sinha, A. Bhaumik, Catal. Commun. 10 (2009) 2041–2045.
[46] P.I. Ravikovitch, A.V. Neimark, J. Phys. Chem. B 105 (2001) 6817–6823.
[47] C.-T. Wang, J.-C. Lin, Appl. Surf. Sci. 254 (2008) 4500–4507.
[48] S.K. Das, M.K. Bhunia, A. Bhaumik, Dalton Trans. 39 (2010) 4382–4390.
[49] W.H. Zhang, J.L. Shi, L.Z. Wang, D.S. Yan, Chem. Mater. 12 (2000) 1408–1413.
[50] L.Q. Wang, H.M. Kang, D.F. Xue, C.H. Liu, J. Crystal Growth 311 (2009) 611–614.
[51] C. Ye, Y. Wang, Y. Ye, J. Zhang, G.H. Li, J. Appl. Phys. 106 (2009) 033520.
[52] NMR data of pamitic acid methyl ester: 1H NMR (300 MHz, CDCl3): (0.794–0.822 (t, 3H), 1.158–1.235 (m, 24H), 1.545–1.560 (m, 2H), 2.252–2.267 (t, 2H), 3.662 (s, 3H). 13C NMR (500 MHz, CDCl3): (14.25, 18.57, 22.84, 24.91, 29.4–29.83 (9C), 32.08, 33.77, 58.63, 171.49. Oleic acid methyl ester: 1H NMR (300 MHz, CDCl3): (0.82–0.85(t, 3H), 1.20–1.30 (m, 19H), 1.56–1.59 (m, 2H), 1.95–1.98(m, 4H), 2.24–2.26 (t, 2H), 3.61(s, 3H), 5.28–5.30 (m, 2H). 13C NMR (500 MHz, CDCl3): (14.2, 22.6, 24.9, 25.7, 29.1–29.8 (8C), 31.6, 31.9, 34.1, 51.3, 130.1-128.1 (2C), 174.2. Lauric acid methyl ester: 1H NMR (300 MHz, CDCl3): (0.82–0.85(t, 3H), 1.22–1.25 (m, 16H), 1.55–1.61 (m, 2H), 2.25–2.30 (m, 2H), 3.43, 3.63 (s, 3H). 13C NMR (500 MHz, CDCl3): (14.1, 22.7, 25.0, 29.2-29.7 (6C), 31.9, 34.1, 50.6, 179.1. %Conversion was estimated from 1H NMR: [Peak area of one proton near 3.6 (for –CH3 gr.) divided by that of one proton at 2.25 (–CH2 gr.)] × 100.